Budgets of Reynolds Stresses and Turbulent Heat Flux for Hypersonic Turbulent Boundary Layers Subject to Pressure Gradients

Gary L. Nicholson*, Junji Huang† and Lian Duan‡
The Ohio State University, Columbus, OH 43210

Meelan M. Choudhari§
NASA Langley Research Center, Hampton, VA 23681

Bryan Morreale¶, Rodney D.W. Bowersox‖
Texas A&M University, College Station, TX 77843

In this paper, the budget terms in the transport equations of the Reynolds stresses, the turbulent kinetic energy (TKE), the internal energy, and the turbulent heat flux are computed using a direct numerical simulation (DNS) database of hypersonic turbulent boundary layers (TBLs) subject to favorable pressure gradients (FPG). Study of the Reynolds stress and TKE budgets shows that FPG has a damping effect on turbulence production, transport, and destruction. The semilocal scaling fails to collapse the Reynolds stress and TKE budget terms between the zero pressure gradient (ZPG) and the strong FPG cases, suggesting that the mechanical nonequilibrium due to FPG leads to changes in Reynolds stress and TKE transport that cannot be captured by Morkovin's hypothesis. Minimal change is seen in the internal energy budget in the presence of FPG, indicating a minimal impact due to FPG on the mean thermal field. While the near-wall transport of wall-normal turbulent heat flux is largely governed by the balance between the turbulent viscous-thermal transport term and the turbulent viscous-thermal dissipation term, the transport of the streamwise turbulent heat flux is influenced by contributions from almost all the budget terms. For the strong FPG case in particular, production due to both the mean and the fluctuating strain rates begins to play a significant role in the near-wall transport of the streamwise turbulent heat flux, and their inclusion or modeling may be required to accurately predict turbulent heat fluxes for a strong FPG.

Nomenclature

B_q	=	wall heat transfer rate, $B_q = q_w/(\rho_w C_p u_\tau T_w)$, dimensionless
C_f	=	wall skin friction coefficient, $C_f = \tau_w/(\frac{1}{2}\rho_\infty U_\infty^2)$, dimensionless
C_h	=	wall heat flux coefficient, $C_h = q_w/\left(\rho_\infty C_p U_\infty (T_r - T_w)\right)$, dimensionless
C_p	=	heat capacity at constant pressure, J/(K·kg)
C_v	=	heat capacity at constant volume, J/(K·kg)
E	=	total energy per unit mass, $E \equiv e + \frac{1}{2}u_i u_i$, J/kg
H	=	shape factor, $H \equiv \delta^*/\theta$, dimensionless
M	=	Mach number, $M \equiv u/a$, dimensionless
M_τ	=	friction Mach number, $M_\tau = u_\tau/(\gamma R T_w)^{1/2}$, dimensionless
N_f	=	number of fields used to accumulate statistics, dimensionless
Pr	=	molecular Prandtl number, $Pr = 0.71$, dimensionless

*Graduate Student, Department of Mechanical and Aerospace Engineering, Student Member, AIAA
†Graduate Student, Department of Mechanical and Aerospace Engineering, Student Member, AIAA
‡Associate Professor, Department of Mechanical and Aerospace Engineering, Associate Fellow, AIAA
§Aerospace Technologist, Computational AeroSciences Branch, M.S. 128. Fellow, AIAA
¶Graduate Student, Department of Aerospace Engineering, Student Member, AIAA
‖Associate Dean for Research, Ford Motor Co. Design Professor, Fellow, AIAA

Pr_t = turbulent Prandtl number, $Pr_t \equiv \left(\overline{\rho u'' w''}(\partial \tilde{T}/\partial z)\right) / \left(\overline{\rho w'' T''}(\partial \tilde{u}/\partial z)\right)$, dimensionless

R = ideal gas constant, $R = 287$, J/(K·kg)

Re_θ = Reynolds number based on momentum thickness and freestream viscosity, $Re_\theta \equiv \rho_\infty u_\infty \theta/\mu_\infty$, dimensionless

$Re_{\delta 2}$ = Reynolds number based on momentum thickness and wall viscosity, $Re_{\delta_2} \equiv \rho_\infty u_\infty \theta/\mu_w$, dimensionless

Re_τ = Reynolds number based on shear velocity and wall viscosity, $Re_\tau \equiv \rho_w u_\tau \delta/\mu_w$, dimensionless

Re^*_τ = semilocal Reynolds number, $Re^*_\tau \equiv \sqrt{\tau_w/\rho_\infty}\delta/\nu_\infty$, dimensionless

T = temperature, K

T_r = recovery temperature, $T_r = T_\infty(1 + 0.89\frac{\gamma-1}{2}M^2_\infty)$, K

T_f = time spanned to accumulate statistics, s

U_∞ = freestream velocity, m/s

a = speed of sound, m/s

e = internal energy per unit mass, $e \equiv C_v T$, J/kg

h = enthalpy per unit mass, $h \equiv C_p T$, J/kg

$\widetilde{k}$ = turbulent kinetic energy, $\widetilde{k} \equiv \widetilde{u''_i u''_i}/2$, J/kg

p = pressure, Pa

q = conductive heat flux, W/m^2

q^T_i = turbulent heat flux term, $q^T_i = \overline{\rho h'' u''_i}$, W/m^2

q_w = wall heat flux, W/m^2

s = entropy, J/(kg·K)

u = streamwise velocity in the local body intrinsic coordinate system, m/s

u_τ = friction velocity, $u_\tau \equiv \sqrt{\tau_w/\overline{\rho}_w}$, m/s

u^*_τ = density weighted velocity scale, $u^*_\tau \equiv \sqrt{\tau_w/\overline{\rho}} = u_\tau\sqrt{\overline{\rho}_w/\overline{\rho}}$, m/s

v = spanwise velocity in the local body intrinsic coordinate system, m/s

w = wall-normal velocity in the local body intrinsic coordinate system, m/s

x = streamwise direction of the local body intrinsic coordinate system, m

x_g = streamwise direction of the right-handed Cartesian coordinate system, m

y = spanwise direction of the local body intrinsic coordinate system, m

y_g = spanwise direction of the right-handed Cartesian coordinate system, m

z = wall-normal direction of the local body intrinsic coordinate system, m

z_g = vertical coordinate that is perpendicular to the plane determined by the x_g- and y_g-coordinates, m

z_τ = viscous length, $z_\tau = \nu_w/u_\tau$, m

z^*_τ = semilocal length scale, $z^*_\tau \equiv \bar{\mu}/(\bar{\rho}u^*_\tau)$, m

β = Clauser pressure gradient parameter, $\beta = (dp/dx)(\delta^*/\tau_w)$, dimensionless

β_{inc} = incompressible Clauser pressure gradient parameter, $\beta = (dp/dx)(\delta^*_{inc}/\tau_w)$, dimensionless

γ = specific heat ratio, $\gamma = C_p/C_v$, dimensionless

δ = boundary-layer thickness (based on 99.5% of the freestream total enthalpy), m

δ^* = displacement thickness, $\delta^* = \int_0^\delta \left(1 - \frac{\rho u}{\rho_e u_e}\right) dz$, m

δ^*_{inc} = incompressible displacement thickness, $\delta^*_{inc} = \int_0^\delta \left(1 - \frac{u}{u_e}\right) dz$, m

κ = von Kármán constant $\kappa = 0.41$, dimensionless

θ = momentum thickness, $\theta = \int_0^\delta \frac{\rho u}{\rho_e u_e}\left(1 - \frac{u}{u_e}\right) dz$, m

θ_{inc} = incompressible momentum thickness, $\theta_{inc} = \int_0^\delta \frac{u}{u_e}\left(1 - \frac{u}{u_e}\right) dz$, m

ϑ^T_i = turbulent heat flux term, $\vartheta^T_i = \overline{\rho e'' u''_i}$, W/m^2

μ = dynamic viscosity, $\mu = 1.458 \times 10^{-6} T^{3/2}/(T + 110.4)$, kg/(m·s)

ν = kinematic viscosity, $\nu = \mu/\rho$, m^2/s

ρ = density, kg/m^3

S_{ij} = the rate-of-strain tensor, $S_{ij} = \frac{1}{2}(\frac{\partial u_i}{\partial x_j} + \frac{\partial u_j}{\partial x_i})$, Hz

t_{ij} = the viscous stress tensor, $t_{ij} = 2\mu(S_{ij} - \frac{1}{3}S_{kk}\delta_{ij})$, Pa

Subscripts

i = inflow station for the domain of direct numerical simulations
inc = incompressible variables
rms = root mean square
w = wall variables
∞ = freestream variables

Superscripts

T = turbulent quantities in RANS equations
$+$ = variable in inner wall units, $(\cdot)^+ \equiv (\cdot)/z_\tau$
$*$ = variable in semilocal units, $(\cdot)^* \equiv (\cdot)/z_\tau^*$
$\overline{(\cdot)}$ = standard (Reynolds) averaged variable
$\widetilde{(\cdot)}$ = density-weighted (Favre) averaged variable, $\widetilde{(\cdot)} \equiv \overline{\rho(\cdot)}/\overline{\rho}$
$(\cdot)'$ = fluctuations around standard averages
$(\cdot)''$ = fluctuations around Favre averages

I. Introduction

High-fidelity simulations, such as direct numerical simulations (DNS) and large-eddy simulations (LES), can inform the model development by providing detailed, global distributions of turbulent fluctuations, including the desired terms from the turbulent kinetic energy (TKE) and Reynolds-stress budgets as well as other quantities of relevance to turbulence modeling. In the past, investigations of TKE and Reynolds-stress budgets in the supersonic and hypersonic regime have been carried out via DNS studies of flat-plate, zero-pressure-gradient (ZPG) turbulent boundary layers (TBLs) [1–6], channel and pipe flows [7–10], as well as shock wave/boundary-layer interactions [11–14].

In regard to the modeling of the turbulent heat flux for high-speed shear flows, Bowersox [15, 16] derived an algebraic energy flux (AEF) model by truncating the transport equation for the turbulent heat flux. The newly developed turbulent energy flux model showed significant improvements over the constant Prandtl number model, up to 20% in the temperature predictions for boundary-layer flows over moderately cooled walls with $T_w/T_r > 0.3$ [15–17]. More recently, the present authors extended the assessment of Bowersox's AEF model to zero-pressure-gradient TBLs at Mach 11 and 14, each with a highly-cooled wall corresponding to $T_w/T_r \cong 0.2$ [18]. They found that the AEF model improves the prediction of the temperature profiles over the commonly used constant-Pr_t formulation, while maintaining a good prediction of the velocity field in the hypersonic cold-wall regime. So far, the assessment of the AEF model has been limited to turbulent boundary layers with ZPG. Therefore, a detailed study of the budget terms from the transport equations for the Reynolds stress and the turbulent heat flux is critical to extending the usage of this model to turbulent boundary layers subject to either favorable and/or adverse pressure gradients.

Recently, Nicholson et al. [19] presented the findings based on a new, in-depth DNS dataset of nominally Mach 5 TBLs subject to favorable pressure gradients (FPG) due to streamline curvature. The DNS simulated the experimental flow configurations performed in the National Aerothermochemistry Laboratory (NAL) at the Texas A&M University (TAMU), including those with zero, weak, and strong favorable pressure gradients that were induced via an appropriately designed surface curvature [20]. The DNS was validated against the experimental results of Tichenor et al. [20] for both zero and nonzero pressure gradients, as well as through selective comparisons with several other DNS datasets for a ZPG boundary layer [21–23]. In general, the DNS results agreed very well with the velocity profiles measured in the experiments. Furthermore, for the ZPG cases, the Van Driest II transformed mean velocity profiles from the DNS showed good collapse with other DNS results for a variety of Mach numbers. Consistent with the experiment by Tichenor et al. [20], the DNS also predicted a substantial reduction in Reynolds stresses and the turbulent heat flux with an increasing pressure gradient. For a sufficiently strong pressure gradient, the shear stress and the wall-normal heat flux became nearly zero or even slightly negative in the outer region of the boundary layer, which may indicate a decaying turbulent motion. The constant-Prandtl-number assumption and Huang's version of strong Reynolds analogy were shown to be adequate for zero and weak pressure gradients, but failed under a strong-pressure-gradient flow.

In addition to characterizing the physics of high-speed turbulence subject to a streamline-curvature-driven FPG, the DNS datasets of Nicholson et al. [19] were used to assess the potential limitations resulting from the modeling assumptions associated with several currently available turbulence models. They found that the Boussinesq assumption provided reasonable predictions of the Reynolds shear stress, but failed to adequately predict the streamwise and

wall-normal Reynolds stresses. While the assumption of a constant turbulent Prandtl number provided good predictions of the turbulent heat flux in the wall-normal direction, it failed to capture the turbulent heat transfer in the streamwise direction. These previous results suggest a requirement for higher-fidelity models that can successfully capture the transport of Reynolds stresses and turbulent heat fluxes in all coordinate directions. An assessment of the budget terms from the transport equations for the TKE, the Reynolds stresses, and the turbulent heat flux in hypersonic TBLs with nonzero pressure gradients will shed further light on the development of physics based high-fidelity models.

The primary objective of this paper is to evaluate the budget terms of the transport equations for TBLs developing under favorable pressure gradients by using the existing DNS database from Nicholson et al. [19], including the budgets of the Reynolds stress, the TKE, the internal energy, and the turbulent heat flux. In particular, the current study extends the assessment of several modeling assumptions from the AEF model to the case of high-speed TBLs subject to nonzero pressure gradients. We also seek a further improvement of this model on the basis of the information derived from the budget terms.

The paper is structured as follows. The flow conditions and numerical methodology are outlined in Section II. Section III presents the results for the budget terms for the Reynolds stress, the TKE, the internal energy, and turbulent heat flux. A summary of the paper is given in Section IV.

II. Flow Conditions and Numerical Methodology

In the present work, the Reynolds stress and turbulent heat flux budgets of TBLs subject to pressure gradients are studied by using a DNS database of nominally Mach 5 TBLs subject to pressure gradients due to streamline curvature [19]. The flow conditions and the wall geometry were selected to closely match those from the experiment by Tichenor et al. [20] in the NAL at the TAMU. The wall geometry in their experiment consisted of a tunnel wall with a changeable floor insert that could be varied from a flat wall with zero pressure gradient to a curved surface that induced a favorable pressure gradient. Table 1 outlines the freestream and wall-temperature conditions for the current DNS. Three DNS were performed to simulate the TBLs developing spatially under the three different pressure gradient distributions considered in the experiment: ZPG, weak pressure gradient (WPG), and strong pressure gradient (SPG). Specifically, Case M5ZPG simulated a baseline ZPG TBL over a flat plate, and Cases M5WPG and M5SPG simulated TBLs over curved-wall geometries that produced weak and strong favorable pressure gradients (FPGs), respectively. The curved wall geometries were prescribed in Cases M5WPG and M5SPG by the following polynomial profile:

$$z_{g,w}(x_g) = A(x_g - x_{g,1})^3 + B(x_g - x_{g,1})^2 \quad (m), \quad (x_{g,1} \le x_g \le x_{g,2}) \tag{1}$$

where $x_{g,1} = 0.2454$ m was the global axial location where the curvature began, and A and B were polynomial coefficients ($A = 0.642$ and $B = -0.3757$ for Case M5WPG, and $A = 11.07$ and $B = -2.507$ for Case M5SPG). The positions where the curvature ended for the Cases M5WPG and M5SPG were given by $x_{g,2} = 0.6354$ m and $x_{g,2} = 0.3964$ m, respectively. These curved wall geometries were the same as those of the two favorable-pressure-gradient models investigated during the TAMU experiment. Figure 1 provides a schematic for each of the DNS cases. The two sample locations to be studied in detail matched those in Tichenor et al. [20], including $x_g = 0.159$ m, labeled as location 1, and $x_g = 0.298$ m, labeled as location 2. Here, location 1 is representative of a ZPG TBL, while location 2 is within the curved wall regions to allow the effects of a nonzero pressure gradient to be assessed.

DNS of the high-speed turbulent boundary layers were performed by solving the compressible Navier-Stokes equations in conservation form. The inviscid fluxes of the governing equations in curvilinear coordinates were computed by using a seventh-order weighted essentially nonoscillatory (WENO) scheme. The viscous fluxes were discretized with a fourth-order central difference scheme and time integration was performed using a third-order low-storage Runge-Kutta scheme [24]. Figure 2 shows the computational domain for the Cases M5WPG and M5SPG. The computations were carried out in three stages involving overlapping streamwise domains. The Box 1 and Box 2 DNS simulated a ZPG TBL over a flat plate, and only the Box 3 DNS simulated the TBLs over a curved wall geometry that produced either a weak or a strong FPG. For each wall shape, no-slip conditions were applied for the three velocity components at the wall, and an isothermal condition was used for the temperature, with $T_w = 317$ K. At the top and the outflow boundaries, unsteady non-reflecting boundary conditions based on Thompson [25] were imposed, and periodic boundary conditions were used in the spanwise direction. The accuracy of the DNS has been addressed by performing checks which ensured that any sensitivity to the grid resolution is suitably small, as well as via comparisons with the available measurements from the wind tunnel experiments. For additional details of the numerical methods and the validation of the DNS against experiments, the reader is deferred to Nicholson et al. [19].

Table 1 Freestream and wall-temperature conditions for the nominally Mach 5 DNS cases of Nicholson et al. [19]. δ_i **is the boundary-layer thickness at the inflow of Box 1 DNS (**$x_g = -0.163$ **m) as shown in Figure 2.**

Case	M_∞	U_∞, m/s	ρ_∞, kg/m^3	T_∞, K	T_w, K	T_w/T_r	T_r	δ_i, mm
DNS	4.9	794.0	0.272	66.2	317.0	0.91	348	4.0

Table 2 Boundary-layer properties at the sample stations, Location 1 ($x_g = 0.159$ **m) and Location 2 (**$x_g = 0.298$ **m), selected for the analysis for the DNS cases.**

Dataset	x_g, m	Re_θ	Re_τ	$Re_{\delta 2}$	Re^*_τ	θ, mm	H_{12}	δ, mm	z_τ, μm	u_τ, m/s	β	β_{inc}
M5ZPG	0.159	17406	882	4021	6854	0.358	10.4	7.8	8.89	38.1	≈ 0	≈ 0
M5WPG	0.298	19178	934	4429	7691	0.395	13.7	9.7	10.5	38.3	-1.09	-0.24
M5SPG	0.298	27988	645	6464	6668	0.576	18.0	12.6	19.6	40.5	-5.71	-0.9

III. Budgets for FPG Turbulent Boundary Layers

In this section, results from the DNS database of Nicholson et al. [19] are investigated to find the impact of favorable pressure gradients on the budget terms in several transport equations, including those of the Reynolds stress (Section III.A), the TKE (Section III.B), the internal energy (Section III.C), and the turbulent heat flux (Section III.D). For reference, Table 2 lists the boundary layer properties at each sample location, including the values of various Reynolds number parameters and the Clauser pressure gradient parameter $\beta = (dp/dx)(\delta^*/\tau_w)$.

A. Reynolds-stress budgets

The Favre-averaged Reynolds-stress tensor is defined as $\overline{\rho}\widetilde{\tau}_{ij} = \overline{\rho u_i'' u_j''}$, and its transport equation has the following form [26]:

$$\overline{\rho}\frac{D\widetilde{\tau}_{ij}}{Dt} = \frac{\partial(\overline{\rho}\widetilde{\tau}_{ij})}{\partial t} + \frac{\partial}{\partial x_k}\left(\overline{\rho}\widetilde{\tau}_{ij}\widetilde{u}_k\right) = P_{ij} + T_{ij} + \Pi_{ij} - \overline{\rho}\epsilon_{ij} + D_{ij} + M_{ij} \tag{2}$$

where,

$$\begin{aligned}
P_{ij} &= -(\overline{\rho}\widetilde{\tau}_{ik}\frac{\partial \widetilde{u}_j}{\partial x_k} + \frac{\partial \widetilde{u}_i}{\partial x_k}\overline{\rho}\widetilde{\tau}_{jk}) = -(\overline{\rho u_i'' u_k''}\frac{\partial \widetilde{u}_j}{\partial x_k} + \frac{\partial \widetilde{u}_i}{\partial x_k}\overline{\rho u_k'' u_j''}) \\
T_{ij} &= -\frac{\partial}{\partial x_k}(\overline{\rho u_i'' u_j'' u_k''}) \\
\Pi_{ij} &= -\overline{(u_i''\frac{\partial p'}{\partial x_j} + u_j''\frac{\partial p'}{\partial x_i})} \\
\overline{\rho}\epsilon_{ij} &= \overline{t'_{ik}\frac{\partial u_j''}{\partial x_k}} + \overline{t'_{jk}\frac{\partial u_i''}{\partial x_k}} \\
D_{ij} &= \frac{\partial}{\partial x_k}(\overline{t'_{ik}u_j'' + t'_{jk}u_i''}) \\
M_{ij} &= \overline{u_i''}\left(\frac{\partial \overline{t}_{kj}}{\partial x_k} - \frac{\partial \overline{p}}{\partial x_j}\right) + \overline{u_j''}\left(\frac{\partial \overline{t}_{ki}}{\partial x_k} - \frac{\partial \overline{p}}{\partial x_i}\right).
\end{aligned} \tag{3}$$

The transport of the turbulent stress is shown to be controlled by a balance among the production term P_{ij}, the turbulent transport term T_{ij}, the velocity pressure-gradient term Π_{ij}, the viscous dissipation term $\overline{\rho}\epsilon_{ij}$, the viscous diffusion term D_{ij}, and the mass flux contribution term M_{ij}.

Figure 3 plots the budget terms for the streamwise Reynolds stress ($\tau_{11} = \overline{\rho u'' u''}/\overline{\rho}$), wherein each term is normalized by the semilocal scaling $\overline{\rho}u_\tau^{*3}/z_\tau^*$. For the cases with zero and weak pressure gradients, the streamwise production term P_{11} shows a near-wall peak around $z^* = 12$, while the peak has shifted slightly outward to $z^* \approx 14$ in the SPG case. In

the meantime, the magnitude of the peak production has also reduced for the SPG case. The turbulent diffusion term T_{11} shows a similar reduction in the peak magnitude at $z^* \approx 15$ for the SPG case. For all cases, the viscous diffusion term D_{11} and the viscous dissipation term $\overline{\rho}\epsilon_{11}$ nearly balance each other within the viscous sublayer ($z^* \lesssim 5$). However, the magnitude of both terms is significantly smaller in the SPG case, similar to the production term P_{11}. The velocity pressure-gradient term Π_{11} is nearly zero everywhere except for the buffer layer, where it has slightly negative values. FPGs lead to a reduction in the magnitude of Π_{11} and, consequently, a further weakened redistribution of the turbulent energy from the streamwise component to the other two components. The turbulent mass flux term M_{11} is nearly zero across the entire boundary layer and therefore can be neglected in the context of turbulence modeling [27].

Figures 4 and 5 plot the budget terms of the transport equation for the spanwise and wall-normal Reynolds stresses ($\tau_{22} = \overline{\rho v'' v''}/\overline{\rho}$ and $\tau_{33} = \overline{\rho w'' w''}/\overline{\rho}$, respectively). The production term (P_{22} or P_{33}) almost vanishes or even becomes slightly negative in the near wall region. Instead, the velocity pressure-gradient term (Π_{22} or Π_{33}) becomes the dominant source of these two Reynolds stress components. As the favorable pressure gradient is increased, the velocity pressure-gradient term (Π_{22} or Π_{33}) decreases modestly, indicating a commensurate reduction in the redistribution of turbulent energy from the streamwise direction to the spanwise and wall-normal directions. While the spanwise turbulent transport term T_{22} is small compared to the other terms, the wall-normal turbulent transport term T_{33} displays a complex variation including both positive and negative peaks in the near wall region. Similar to the velocity pressure-gradient term, the strong favorable pressure gradient leads to a reduction in the peak magnitudes of the turbulent transport term (T_{22} or T_{33}), the viscous dissipation term ($\overline{\rho}\epsilon_{22}$ or $\overline{\rho}\epsilon_{33}$), and the viscous diffusion term (D_{22} or D_{33}). The mass-transport term (M_{22} or M_{33}) for both the spanwise and wall-normal Reynolds stresses is negligibly small throughout the boundary layer, similar to the M_{11} term for the streamwise Reynolds stress.

Figure 6 shows the budget terms for the Reynolds shear stress $\tau_{13} = \overline{\rho u'' w''}/\overline{\rho}$. Within the viscous sublayer, the transport of the Reynolds shear stress is dominated by a balance between the viscous diffusion term D_{13} and the viscous dissipation term $\overline{\rho}\epsilon_{13}$. However, both of these terms become small within the buffer layer, wherein the shear-stress transport is largely governed by a balance among the production term P_{13}, the velocity pressure gradient correlation term Π_{13}, and the turbulent transport term T_{13}. A strong favorable pressure gradient was found to significantly reduce the peak amplitudes of each of these budget terms.

The overall lack of collapse in the budget terms of the Reynolds stresses τ_{ij} between ZPG and SPG cases suggests that a strong FPG tends to produce a significant mechanical nonequilibrium, leading to changes in Reynolds stress transport that cannot be captured by Morkovin's hypothesis.

B. Turbulent Kinetic Energy Budget

The transport equation for the TKE ($\overline{\rho}\widetilde{k} = \overline{\rho u_i'' u_i''}/2$) is given by [27]:

$$\frac{\overline{\rho} D\widetilde{k}}{Dt} = P + T + \Pi - \overline{\rho}\epsilon + D + M \tag{4}$$

where

$$P = -\overline{\rho u_i'' u_k''}\frac{\partial \widetilde{u_i}}{\partial x_k} \tag{5a}$$

$$\mathrm{T} = -\frac{\partial}{\partial x_k}\left(\frac{1}{2}\overline{\rho u_i'' u_i'' u_k''}\right) \tag{5b}$$

$$\Pi = \pi^t + \pi^d = -\frac{\partial}{\partial x_i}(\overline{p' u_i''}) + \overline{p'\frac{\partial u_i''}{\partial x_i}} \tag{5c}$$

$$\overline{\rho}\epsilon = \overline{t'_{ik}\frac{\partial u_i''}{\partial x_k}} \tag{5d}$$

$$D = \frac{\partial}{\partial x_k}(\overline{\tau'_{ik} u_i''}) \tag{5e}$$

$$M = \overline{u_i''}\left(\frac{\partial \overline{\tau_{ik}}}{\partial x_k} - \frac{\partial \overline{p}}{\partial x_i}\right) - \overline{\rho}\widetilde{k}\frac{\partial \widetilde{u_k}}{\partial x_k}. \tag{5f}$$

Here, each budget term is defined in a similar way as that in the Reynolds stress transport equation. Figure 7 shows that the transport of TKE in the viscous sublayer is governed by a balance between the viscous dissipation term $\rho\epsilon$ and the

viscous diffusion term D, while the net production of TKE in the buffer layer is dominated by the interplay between the production term P, the destruction due to the turbulence transport T, the viscous dissipation $\overline{\rho}\epsilon$, and the viscous diffusion D. While the velocity pressure-gradient term had a significant impact on the transport of the normal and shear components of the Reynolds stress, that term is almost zero across the entire boundary layer in Fig. 7. Again, the strong mean pressure gradient is found to significantly reduce the production, dissipation, and transport processes of the TKE, and this reduction is consistent with the previously discussed trend for the Reynolds stress budgets. A similar reduction in the TKE production and dissipation terms due to strong favorable pressure gradients was reported by Wang et al. [28] at a lower, supersonic Mach number of 2.9.

C. Internal Energy Budget

The transport equation for the internal energy budget $\widetilde{e}$ is given by [7]:

$$\frac{\partial \overline{\rho}\widetilde{u_k}\widetilde{e}}{\partial x_k} = \phi_m + \phi_t + D_M + D_T + \Pi_M^d + \Pi_T^d \tag{6}$$

where

$$\phi_m = \overline{t_{ik}}\frac{\partial \overline{u_i}}{\partial x_k} \tag{7a}$$

$$\phi_T = \overline{t'_{ik}\frac{\partial u'_i}{\partial x_k}} \tag{7b}$$

$$D_M = -\frac{\partial \overline{q_k}}{\partial x_k} \tag{7c}$$

$$D_T = -\frac{\partial \overline{\rho} c_v \widetilde{u''_k T''}}{\partial x_k} \tag{7d}$$

$$\Pi_M^d = -\overline{p}\frac{\partial \overline{u_k}}{\partial x_k} \tag{7e}$$

$$\Pi_T^d = -\overline{p'\frac{\partial u'_k}{\partial x_k}}. \tag{7f}$$

Here, ϕ_m and ϕ_T are the mean and turbulent viscous dissipation terms, respectively, D_m and D_T are the molecular and turbulent heat flux gradient terms, respectively, and Π_M^d and Π_T^d are the mean and turbulent pressure dilation terms, respectively. As shown by Huang et al. [7], the terms ϕ_m and Π_M^d represent an exchange between the internal energy and the mean kinetic energy, while ϕ_T and Π_T^d represent an exchange of energy between the internal energy and the turbulent kinetic energy. Figure 8 displays the profiles of each of the aforementioned internal energy budget terms. In the viscous sublayer, the dynamics of the internal energy transport is largely governed by a balance between the mean viscous dissipation and the molecular heat flux gradient terms. As noted with the TKE budgets, the primary effect of the pressure gradient within this region is a mild reduction of the turbulent viscous dissipation. Farther away from the wall in the buffer layer, the internal energy transport is dominated by a balance between the molecular and turbulent heat flux gradient terms. Compared with the Reynolds stress and TKE budgets, one observes a significantly improved collapse of the internal energy budget terms among the three pressure gradient cases, which indicates that the influence of the favorable pressure gradient is largely mechanical, i.e., limited to the velocity field, and its impact on the thermal field is relatively small.

D. Turbulent Heat Flux Budgets

The transport equation for the turbulent heat flux $\overline{\rho T'' u_i''}$ is written as follows:

$$\frac{\partial \overline{\rho T'' u_i''}}{\partial t} + \frac{\partial \overline{\rho T'' u_i''}\widetilde{u}_k}{\partial x_k} = P_{Tu_i}^1 + P_{Tu_i}^2 + \Pi_{Tu_i} - \overline{\rho}\epsilon_{Tu_i} + D_{Tu_i} + C_{Tu_i} \tag{8}$$

where

$$
\begin{aligned}
P^1_{Tu_i} =& -\overline{\rho u_i'' u_k''}\frac{\partial \widetilde{T}}{\partial x_k} - \overline{\rho T'' u_k''}\frac{\partial \widetilde{u}_i}{\partial x_k} - (\gamma-1)\overline{\rho T'' u_i''}\widetilde{S}_{kk} + \frac{1}{c_v}\overline{u_i'' t_{jk}'}\widetilde{S}_{kj} \\
P^2_{Tu_i} =& \frac{1}{c_v}\left(\overline{u_i'' t_{jk}' S_{kj}''} - \overline{u_i'' p' S_{kk}''}\right) \\
\Pi_{Tu_i} =& -\overline{T''\frac{\partial p}{\partial x_i}} \\
\overline{\rho}\epsilon_{Tu_i} =& -\frac{1}{c_v}\overline{q_k'\frac{\partial u_i'}{\partial x_k}} + \overline{t_{ik}'\frac{\partial T'}{\partial x_k}} \\
D_{Tu_i} =& -\frac{\partial \overline{\rho T'' u_i'' u_k''}}{\partial x_k} + \frac{\partial \overline{T' t_{ik}'}}{\partial x_k} - \frac{1}{c_v}\frac{\partial \overline{u_i' q_k'}}{\partial x_k} \\
C_{Tu_i} =& \overline{T''}\frac{\partial \bar{t}_{ik}}{\partial x_k} + \frac{1}{c_v}\left[\overline{u_i'' t}_{jk}\widetilde{S}_{kj} + \overline{u_i'' S_{kj}''}(\bar{t}_{kj} - \overline{p}\delta_{kj})\right].
\end{aligned}
$$

Here, $P^1_{Tu_i}$ is the production due to the mean temperature and velocity gradients, $P^2_{Tu_i}$ is the production due to the fluctuating strain rate, Π_{Tu_i} is the "pressure-scrambling" term, $\overline{\rho}\epsilon_{Tu_i}$ is the turbulent viscous-thermal dissipation term, D_{Tu_i} is the turbulent viscous-thermal transport contribution, and C_{Tu_i} is the term associated with compressibility [29].

Figure 9 plots the budget terms for the streamwise component of the turbulent heat flux. In this figure, each budget term is normalized by $\overline{\rho}u_\tau^{*2}\widetilde{T}/z_\tau^*$ and is plotted as a function of the wall-normal coordinate, z^*, in semilocal units. The transport of the streamwise heat flux is dominated by comparable contributions from almost all of the budget terms. In the viscous sublayer ($z^* \lesssim 5$), the first production term P^1_{Tu} that involves the gradients of the mean temperature and mean velocity fields is found to increase significantly as the favorable pressure gradient becomes stronger, and this increase is balanced by a similar but opposite change in the second production term P^2_{Tu} that is associated with the triple-correlations involving the fluctuating strain rate field. The increase in the magnitude of P^1_{Tu} and P^2_{Tu} for the nonzero pressure gradient cases was found to be caused by a disproportionate reduction in the normalization factor $\overline{\rho}u_\tau^{*2}\widetilde{T}/z_\tau^*$ (equivalent, $\tau_w\widetilde{T}/z_\tau^*$), albeit the absolute magnitudes of both production terms were reduced as a result of FPG. While the turbulent viscous-thermal transport term D_{Tu} and the turbulent viscous-thermal dissipation term $\overline{\rho}\epsilon_{Tu}$ represent the dominant contributors in the viscous sublayer for the ZPG and WPG cases, both production terms (i.e., P^1_{Tu} and P^2_{Tu}) begin to play a significant role in the transport of the streamwise turbulent heat flux for the SPG case. In the buffer to log layer, there is a significant reduction in the magnitude of the production term P^1_{Tu} and the viscous-thermal transport term D_{Tu}, but an increase in the viscous-thermal dissipation term $\overline{\rho}\epsilon_{Tu}$. Minimal changes occur in both the compressibility term C_{tu} and the pressure scrambling term Π_{Tu} due to the effects of the favorable pressure gradients.

As noted above, the first production term $P^1_{Tu_i}$ of the streamwise turbulent heat flux budget is comprised of four different production mechanisms, namely, those involving the mean temperature gradient $\partial\widetilde{T}/\partial x_k$, the mean velocity gradient $\partial\widetilde{u}_i/\partial x_k$, the mean velocity divergence $\widetilde{S}_{kk}$, and the mean strain rate $\widetilde{S}_{kj}$, respectively, while the second production term $P^2_{Tu_i}$ is comprised of two production mechanisms that involve the fluctuating strain rate S''_{kj} and the fluctuating velocity divergence S''_{kk}. Figure 10 shows each of the four production mechanisms in the first production term P^1_{Tu} for cases with and without pressure gradients. The components due to the mean temperature gradient, the mean velocity gradient, and the mean strain rate make significant contributions to the net production term, whereas the contribution from the mean velocity divergence is seen to be negligible. In the ZPG case, the production term is dominated by the contribution from the mean strain rate in the viscous sublayer. Farther away from the wall, the net production term is dominated by the contributions from the mean-velocity and temperature gradients, whereas the contribution from the mean strain rate is no longer important. This finding is consistent with the neglect of the mean strain rate within the derivation of the AEF model [15, 16]. However, the production due to the mean strain rate becomes increasingly significant in the favorable pressure gradient cases, impacting a significant portion of the boundary layer in the SPG case. Neglecting such a contribution may, therefore, lead to inaccurate near-wall behavior for cases with a relatively strong favorable pressure gradient.

Figure 11 further shows that the term involving the fluctuating strain rate S''_{kj} is the only nonnegligible term in the second production term P^2_{tu} of the streamwise turbulent heat flux budget. This term reduces in magnitude with the favorable pressure gradient and even becomes significantly negative for the SPG case. Such a trend suggests that changes in the fluctuating strain rate field may play an important part in reducing the turbulent heat flux for cases with strong

favorable pressure gradients [19]. Similar to the mean strain rate term in $P^1_{tu_i}$, this term was also neglected in deriving the AEF model [15, 16], which may contribute to potential inaccuracies in cases with significant pressure gradient.

Figure 12 plots the budget terms for the wall-normal component of the turbulent heat flux. In the near wall region ($z^* \lesssim 15$), the wall-normal heat flux budget is governed by a balance of the turbulent viscous-thermal transport term D_{Tu} and the turbulent viscous-thermal dissipation term $\overline{\rho}\epsilon_{Tu}$, while all of the other terms are negligible in this region. Farther away from the wall, i.e., in the buffer layer to log layer, the transport of the wall-normal heat flux was governed instead by a balance between the production term due to the mean temperature and velocity gradients P^1_{Tu} and the pressure scrambling term Π_{Tw}. A strong favorable pressure gradient leads to an observable increase in the peak magnitude of the diffusion and dissipation terms, but has a negligible impact on the remaining four terms. Lastly, Figure 13 shows that the production of the wall-normal turbulent heat flux in the buffer to log layer is exclusively driven by the term associated with the mean temperature gradient.

IV. Summary

An existing DNS database of nominally Mach 5 turbulent boundary layers subject to favorable pressure gradients (FPG) up to $\beta_{inc} = -0.9$ [19] was used to examine the budget terms in the transport equations for the Reynolds stress, the TKE, the internal energy, and the turbulent heat flux. The results were compared with the ZPG baseline case to investigate the effects of FPG on the budget terms. This comparison showed that the FPG resulted in reduced magnitudes of the production, diffusion, and dissipation terms from the Reynolds stress budgets in relation to the ZPG case, indicating a reduction in turbulence generation, transport, and destruction due to the FPG. Additionally, the term from the Reynolds stress budget that involves a correlation between the velocity and the pressure-gradient and is responsible for redistributing the turbulence energy among the three coordinate directions also became smaller with an increasing FPG, suggesting that the FPG leads to a weakened redistribution of the turbulence energy. Similar to the Reynolds stress, the production, diffusion, and dissipation terms of the TKE transport were reduced due to FPG. The semilocal scaling failed to provide an overall collapse in the Reynolds stress and the TKE budget terms between the ZPG and the SPG cases, respectively. The lack of collapse suggests that a strong FPG can produce a significant mechanical nonequilibrium, leading to changes in the Reynolds-stress and TKE transport that cannot be captured by Morkovin's hypothesis. In contrast, however, the FPG of up to $\beta_{inc} = -0.9$ resulted in minimal changes in the terms from the internal-energy budget, indicating that the impact of FPG was mostly limited to the velocity field while a substantial impact on the mean thermal field had not yet occurred.

The transport of wall-normal turbulent heat flux in the near-wall region was found to largely governed by the balance between the turbulent viscous-thermal transport term and the turbulent viscous-thermal dissipation term. On the other hand, the transport of the streamwise turbulent heat flux received nonnegligible contributions from almost all terms from the overall budget. In the strong FPG case, in particular, production due to both the mean strain rate and the triple-correlations involving the fluctuating strain rate also began to play a significant role in the near-wall transport of the streamwise turbulent heat flux. While their omissions were justified for ZPG TBLs as shown in the original derivation of the AEF model [15, 16], it may result in an inaccurate near-wall behavior for flows subjected to a significant FPG. Therefore, it is possible that the AEF model would yield improved predictions for cases with a strong FPG if these terms are either included or modeled in some manner.

Acknowledgments

The authors (Gary L. Nicholson, Junji Huang, and Lian Duan) would like to acknowledge financial support by the Office of Naval Research (under grant N00014-20-1-2194, managed by Dr. Eric Marineau) and the National Science Foundation (under grant CBET 2001127, managed by Dr. Ron Joslin). Author M. Choudhari was supported by the NASA Hypersonic Technology Project. Computational resources were provided by the DoD High Performance Computing Modernization Program and the Ohio Supercomputer Center. The views and conclusions contained herein are those of the authors and should not be interpreted as necessarily representing the official policies or endorsements, either expressed or implied, of the funding agencies or the U.S. Government.

References

[1] Guarini, S. E., Moser, R. D., Shariff, K., and Wray, A., "Direct Numerical Simulation of a Supersonic Turbulent Boundary Layer at Mach 2.5," *Journal of Fluid Mechanics*, Vol. 414, 2000, pp. 1–33.

[2] Duan, L., Beekman, I., and Martin, M., "Direct Numerical Simulation of Hypersonic Turbulent Boundary Layers. Part 2. Effect of Wall Temperature," *Journal of Fluid Mechanics*, Vol. 655, 2010, pp. 419–445.

[3] Duan, L., Beekman, I., and Martin, M., "Direct Numerical Simulation of Hypersonic Turbulent Boundary Layers. Part 3. Effect of Mach Number," *Journal of Fluid Mechanics*, Vol. 672, 2011, pp. 245–267.

[4] Duan, L., and Martin, M., "Direct Numerical Simulation of Hypersonic Turbulent Boundary Layers. Part 4. Effect of High Enthalpy," *Journal of Fluid Mechanics*, Vol. 684, 2011, pp. 25–59.

[5] Pirozzoli, S., and Bernardini, M., "Turbulence in Supersonic Boundary Layers at Moderate Reynolds Number," *Journal of Fluid Mechanics*, Vol. 688, 2011, pp. 120–168.

[6] Zhang, C., Duan, L., and Choudhari, M. M., "Direct Numerical Simulation Database for Supersonic and Hypersonic Turbulent Boundary Layers," *AIAA Journal*, Vol. 56, No. 11, 2018, pp. 4297–4311.

[7] Huang, P. G., Coleman, G. N., and Bradshaw, P., "Compressible Turbulent Channel Flows: DNS Results and Modelling," *Journal of Fluid Mechanics*, Vol. 305, 1995, pp. 185–218.

[8] Coleman, G. N., Kim, J., and Moser, R. D., "A Numerical Study of Turbulent Supersonic Isothermal-wall Channel Flow," *Journal of Fluid Mechanics*, Vol. 305, 1995, pp. 159–183.

[9] Trettel, A., and Larsson, J., "Mean Velocity Scaling for Compressible Wall Turbulence with Heat Transfer," *Physics of Fluids*, Vol. 28, No. 2, 2016, p. 026102.

[10] Ghosh, S., Foysi, H., and Friedrich, R., "Compressible Turbulent Channel and Pipe Flow: Similarities and Differences," *Journal of Fluid Mechanics*, Vol. 648, 2010, pp. 155–181.

[11] Pirozzoli, S., and Bernardini, M., "Direct Numerical Simulation Database for Impinging Shock Wave/Turbulent Boundary-layer Interaction," *AIAA Journal*, Vol. 49, No. 6, 2011, pp. 1307–1312.

[12] Morgan, B., Duraisamy, K., Nguyen, N., and Lele, S. K., "Flow Physics and RANS Modelling of Oblique Shock/Turbulent Boundary Layer Interaction," *Journal of Fluid Mechanics*, Vol. 729, 2013, pp. 231–284.

[13] Vyas, M. A., Waindim, M., and Gaitonde, D. V., "Budget of Turbulent Kinetic Energy in a Shock Wave/Boundary-layer Interaction," *AIAA Paper* 2016-3187, 2016.

[14] Vyas, M. A., Yoder, D. A., and Gaitonde, D. V., "Reynolds-stress Budgets in an Impinging Shock Wave/Boundary-layer Interaction," *AIAA Paper* 2018-1299, 2018.

[15] Bowersox, R. D. W., "Extension of Equilibrium Turbulent Heat Flux Models to High-Speed Shear Flows," *Journal of Fluid Mechanics*, Vol. 633, 2009, pp. 61–70.

[16] Bowersox, R. D. W., and North, S. W., "Algebraic Turbulent Energy Flux Models for Hypersonic Shear Flows," *Progress of Aerospace Sciences*, Vol. 46, 2010, pp. 49–61.

[17] Poggie, J., Bisek, N. J., and Gosse, R., "Resolution Effects in Compressible, Turbulent Boundary Layer Simulations," *Computers and Fluids*, Vol. 120, 2015, pp. 57–69.

[18] Huang, J., Nicholson, G. L., Duan, L., Choudhari, M. M., and Bowersox, R. D., "Simulation and Modeling of Cold-Wall Hypersonic Turbulent Boundary Layers on Flat Plate," *AIAA Paper* 2020-0571, 2020.

[19] Nicholson, G., Huang, J., Duan, L., Choudhari, M. M., and Bowersox, R. D., "Simulation and Modeling of Hypersonic Turbulent Boundary Layers Subject to Favorable Pressure Gradients due to Streamline Curvature," *AIAA Paper* 2021-1672, 2021.

[20] Tichenor, N. R., Humble, R. A., and Bowersox, R. D. W., "Response of a Hypersonic Turbulent Boundary Layer to Favourable Pressure Gradients," *Journal of Fluid Mechanics*, Vol. 722, 2013, pp. 187–213.

[21] Duan, L., Choudhari, M. M., and Zhang, C., "Pressure Fluctuations Induced by a Hypersonic Turbulent Boundary Layer," *Journal of Fluid Mechanics*, Vol. 804, 2016, pp. 578–607.

[22] Bernardini, M., and Pirozzoli, S., "Wall Pressure Fluctuations Beneath Supersonic Turbulent Boundary Layers," *Physics of Fluids*, Vol. 23, No. 8, 2011, p. 085102.

[23] Schlatter, P., and Örlü, R., "Assessment of Direct Numerical Simulation Data of Turbulent Boundary Layers," *Journal of Fluid Mechanics*, Vol. 659, 2010, pp. 116–126.

[24] Williamson, J., "Low-Storage Runge-Kutta Schemes," *Journal of Computational Physics*, Vol. 35, No. 1, 1980, pp. 48–56.

[25] Thompson, K. W., "Time Dependent Boundary Conditions for Hyperbolic Systems," *Journal of Computational Physics*, Vol. 68, No. 1, 1987, pp. 1–24.

[26] Gatski, T. B., and Bonnet, J.-P., *Compressibility, Turbulence, and High Speed Flow*, Academic Press, 2013.

[27] Wilcox, D. C., et al., *Turbulence Modeling for CFD, 3rd ed.*, DCW industries La Canada, CA, 2006.

[28] Wang, X., Wang, Z., Sun, M., Wang, Q., and Hu, Z., "Effects of Favorable Pressure Gradient on Turbulence Structures and Statistics of a Flat-Plate Supersonic Turbulent Boundary Layer," *Physics of Fluids*, Vol. 32, No. 2, 2020, p. 025107.

[29] Shahab, M., Lehnasch, G., Gatski, T., and Comte, P., "Statistical Characteristics of an Isothermal, Supersonic Developing Boundary Layer Flow from DNS Data," *Flow, Turbulence and Combustion*, Vol. 86, No. 3-4, 2011, pp. 369–397.

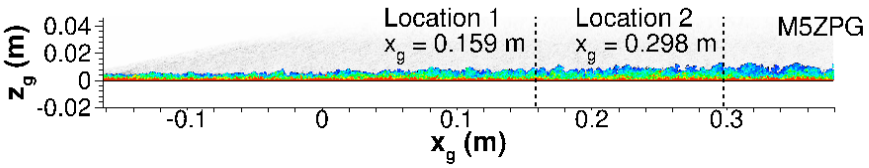

(a) M5ZPG

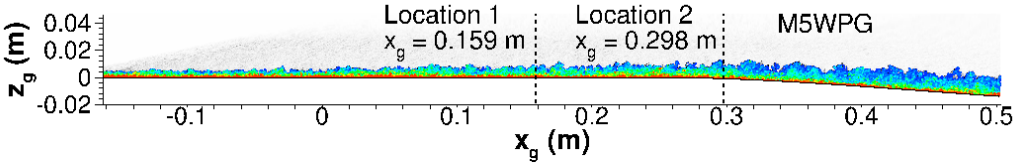

(b) WPG

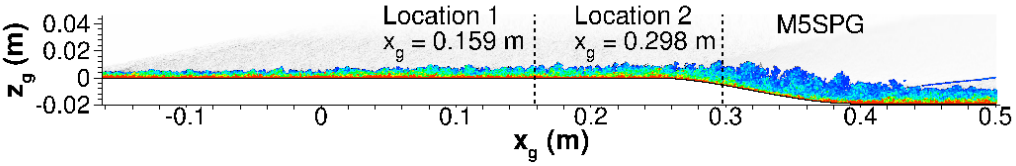

(c) SPG

Fig. 1 Schematic of the DNS cases (a) M5ZPG, (b) M5WPG, and (c) M5SPG. The grey contours are those of numerical schlieren, and the color contours are those of the magnitude of vorticity to highlight the large-scale motions within the boundary-layer. Locations 1 an 2 denote the experiment measurement locations at 0.159 **m and** 0.298 **m, respectively. The curved walls follow the polynomial profile prescribed in Equation 1.**

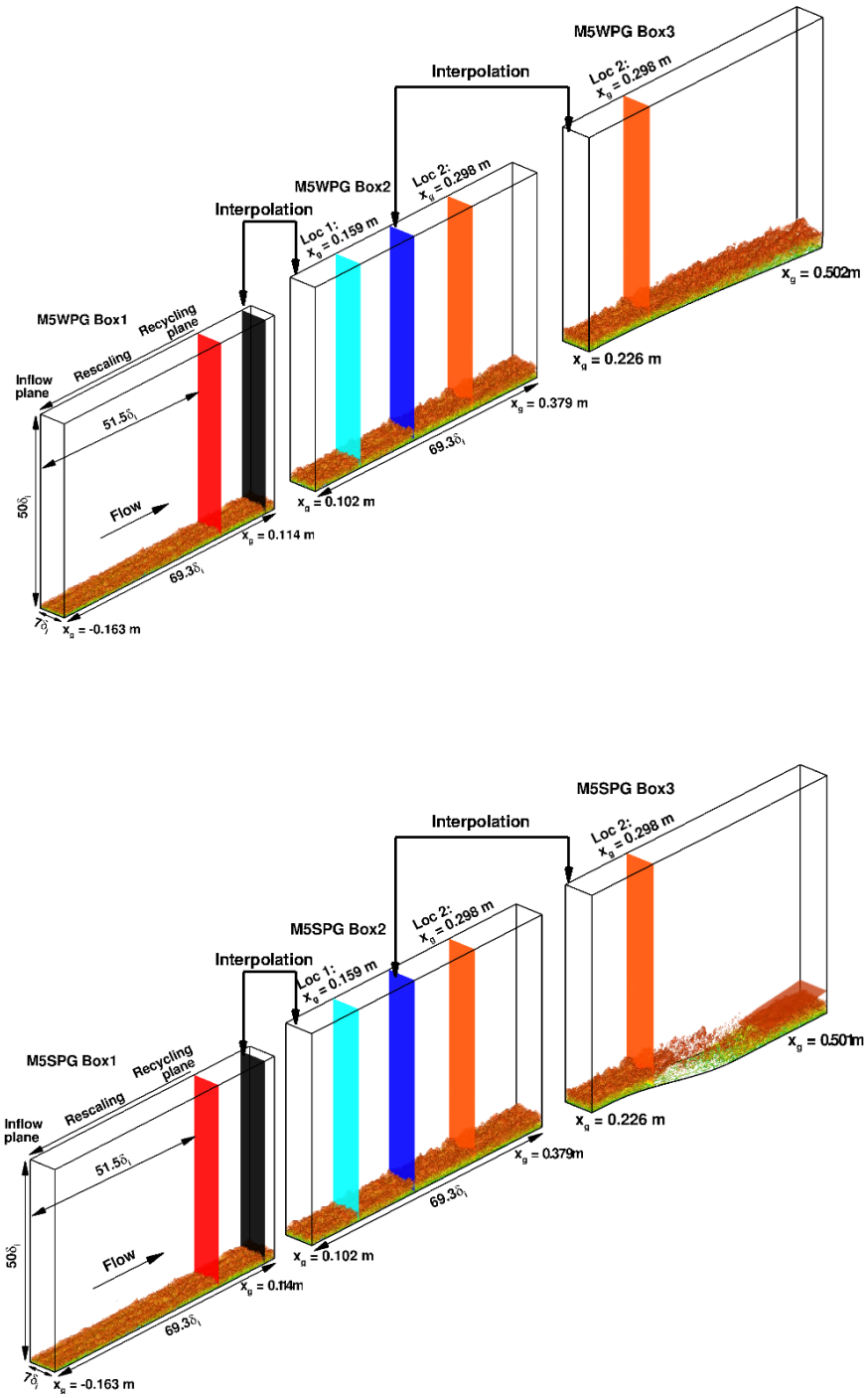

Fig. 2 Computational domain and simulation setup for Mach 5 DNS over wall models of WPG and SPG cases. The instantaneous flow is shown by the isosurface of the magnitude of the density gradient, $|\nabla\rho|\delta_i/\rho_\infty \approx 0.98$ and colored by the streamwise velocity component (with levels from 0 to U_∞, blue to red).

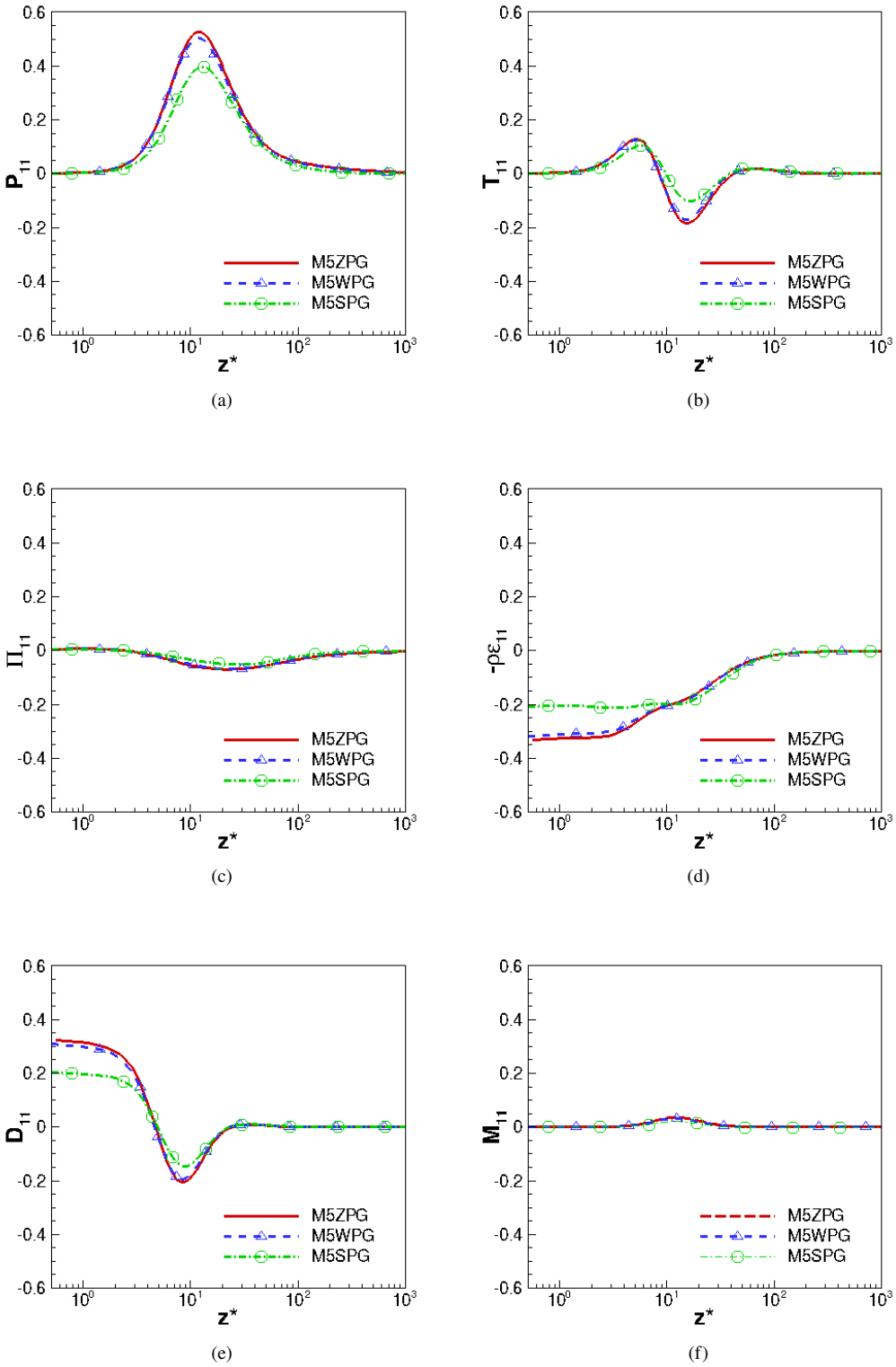

Fig. 3 The streamwise Reynolds-stress budgets $\tau_{11} = \overline{\rho u'' u''}/\overline{\rho}$ of DNS cases with varied pressure gradient: (a) production P_{11}, (b) turbulent diffusion T_{11}, (c) velocity-pressure gradient Π_{11}, (d) viscous dissipation $-\overline{\rho}\epsilon_{11}$, (e) viscous diffusion D_{11}, (f) mass flux contribution M_{11}. Variables are normalized by $\overline{\rho} u_\tau^{*3}/z_\tau^*$ and plotted in semilocal scale z^*. Here, the ZPG profiles are extracted from Location 1, while all other profiles are from Location 2.

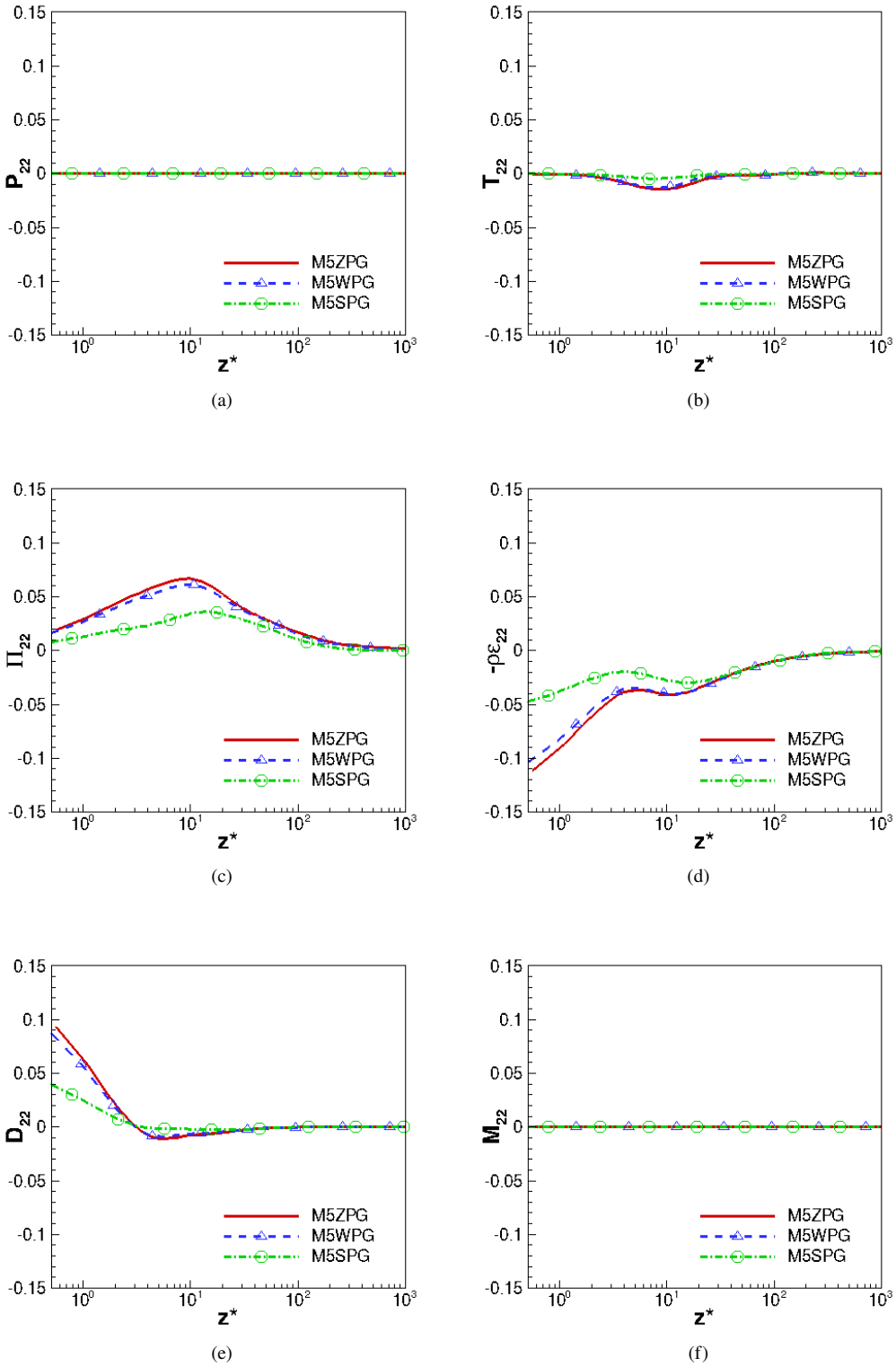

Fig. 4 The spanwise Reynolds-stress budgets $\tau_{22} = \overline{\rho v'' v''}/\overline{\rho}$ of DNS cases with varied pressure gradient: (a) production P_{22}, (b) turbulent diffusion T_{22}, (c) velocity-pressure gradient Π_{22}, (d) viscous dissipation $-\overline{\rho}\epsilon_{22}$, (e) viscous diffusion D_{22}, (f) mass flux contribution M_{22}. Variables are normalized by $\overline{\rho} u_\tau^{*3}/z_\tau^*$ and plotted in semilocal scale z^*. Here, the ZPG profiles are extracted from Location 1, while all other profiles are from Location 2.

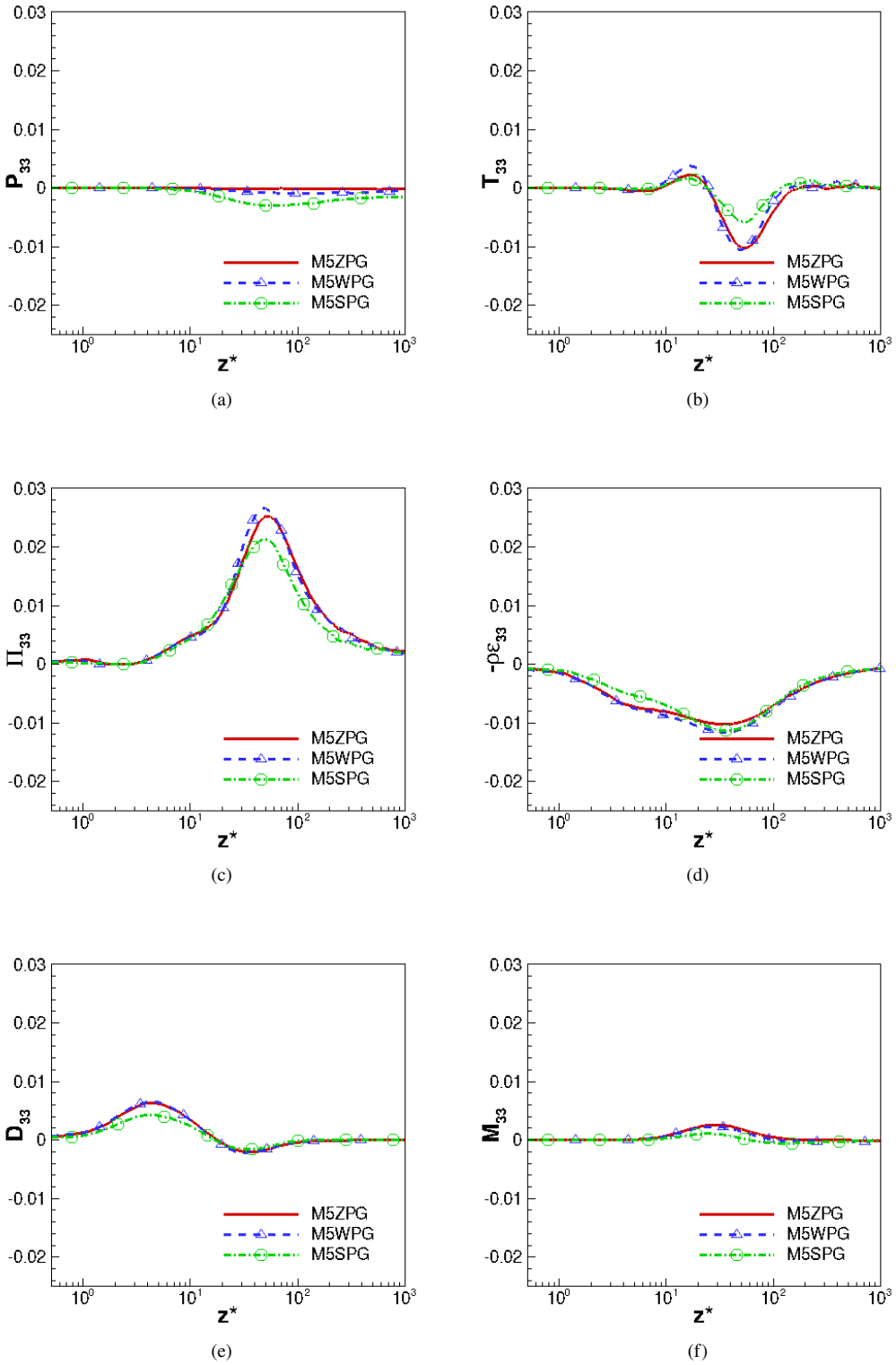

Fig. 5 The wall-normal Reynolds-stress budgets $\tau_{33} = \overline{\rho w'' w''}/\overline{\rho}$ of DNS cases with varied pressure gradient: (a) production P_{33}, (b) turbulent diffusion T_{33}, (c) velocity-pressure gradient Π_{33}, (d) viscous dissipation $-\overline{\rho}\epsilon_{33}$, (e) viscous diffusion D_{33}, (f) mass flux contribution M_{33}. Variables are normalized by $\overline{\rho} u_\tau^{*3}/z_\tau^*$ and plotted in semilocal scale z^*. Here, the ZPG profiles are extracted from Location 1, while all other profiles are from Location 2.

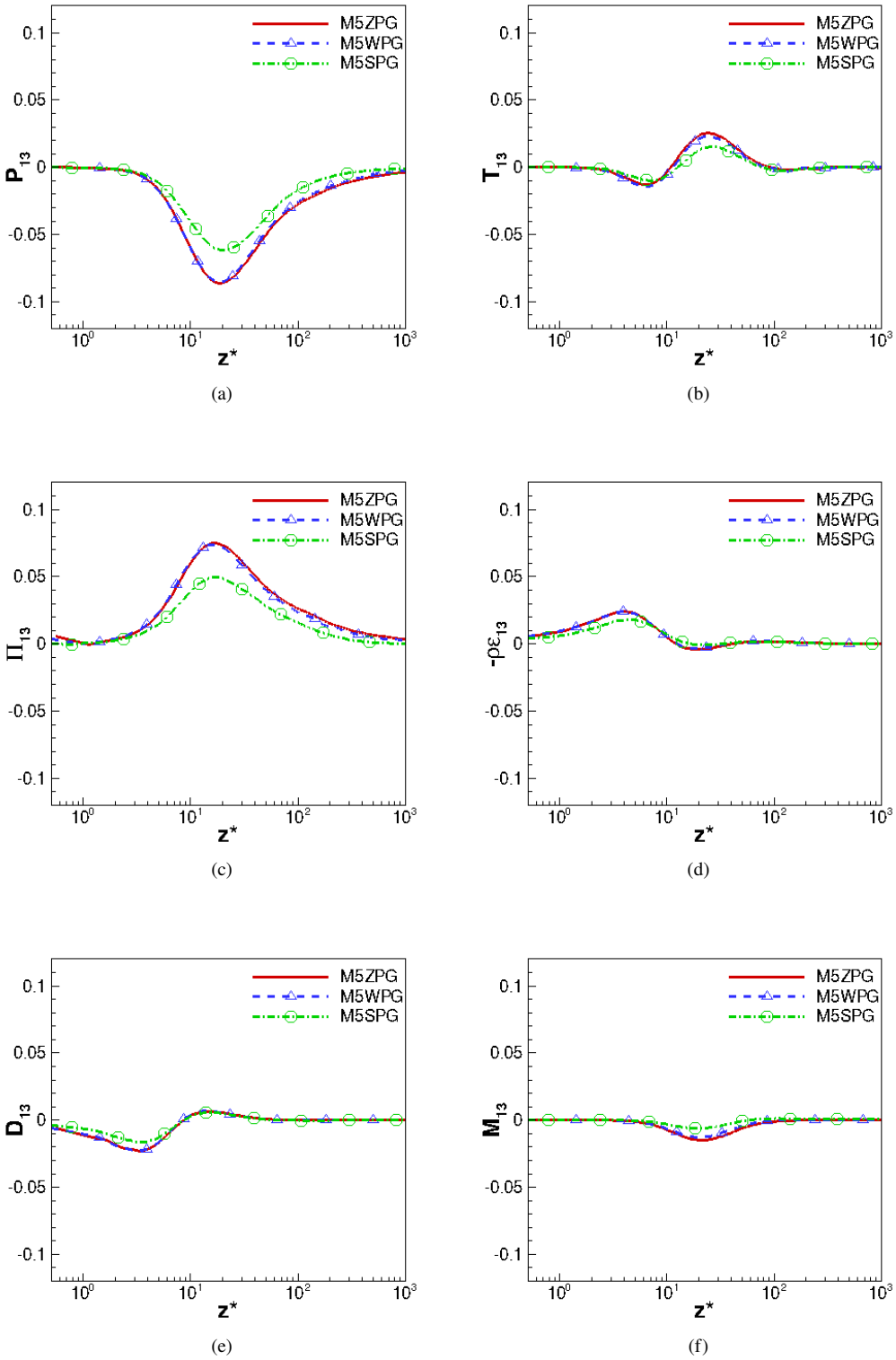

Fig. 6 The Reynolds shear stress budget $\tau_{13} = \overline{\rho u'' w''}/\overline{\rho}$ of DNS cases with varied pressure gradient: (a) production P_{13}, (b) turbulent diffusion T_{13}, (c) velocity-pressure gradient Π_{13}, (d) viscous dissipation $-\overline{\rho}\epsilon_{13}$, (e) viscous diffusion D_{13}, (f) mass flux contribution M_{13}. Variables are normalized by $\overline{\rho} u_\tau^{*3}/z_\tau^*$ and plotted in semilocal scale z^*. Here, the ZPG profiles are extracted from Location 1, while all other profiles are from Location 2.

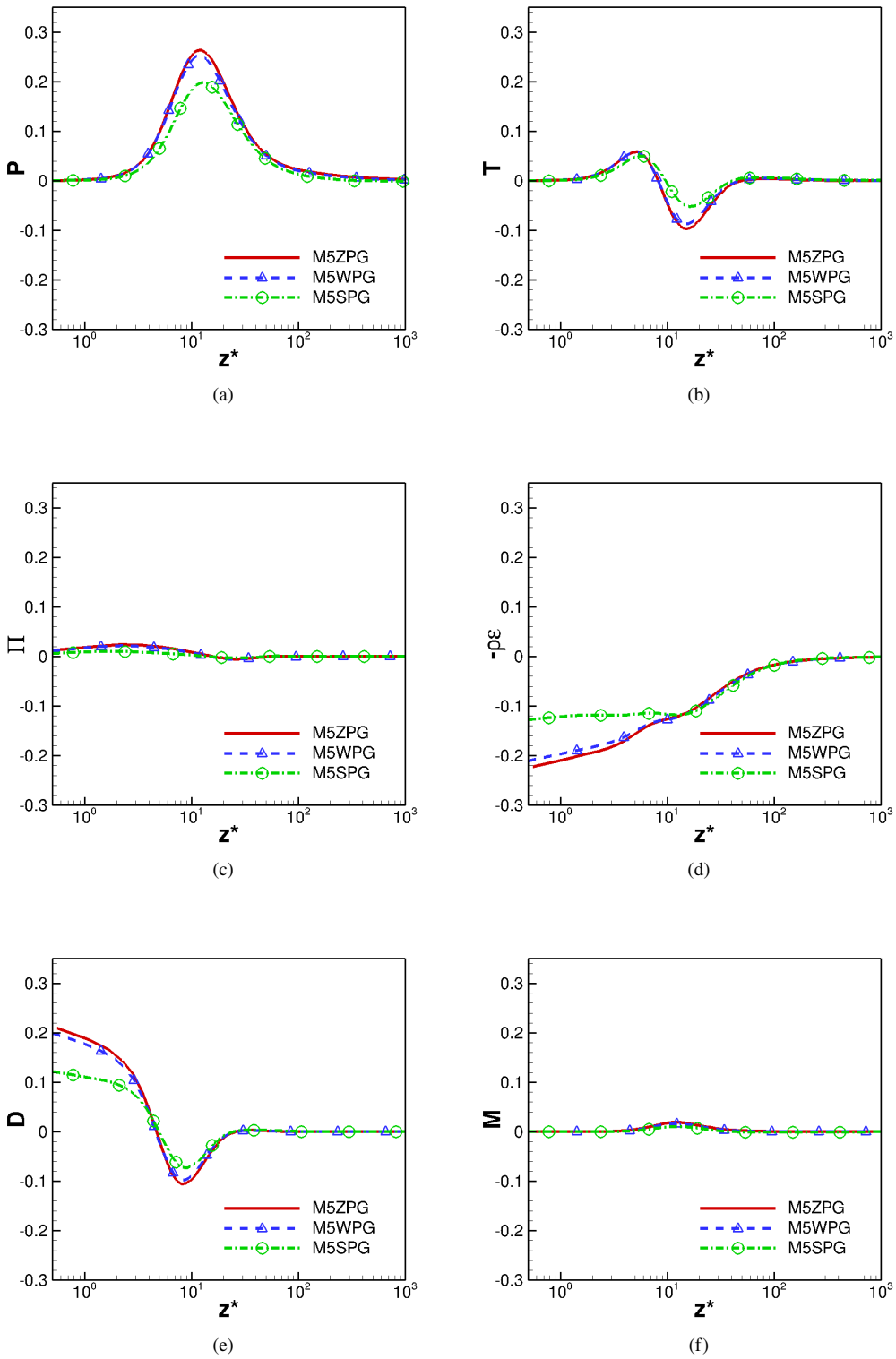

Fig. 7 The TKE budget $k = \frac{1}{2}\overline{\rho u_i'' u_i''}/\overline{\rho}$ of DNS cases with varied pressure gradient: (a) production P, (b) turbulent diffusion T, (c) velocity-pressure gradient Π, (d) viscous dissipation $-\overline{\rho}\epsilon$, (e) viscous diffusion D, (f) mass flux contribution M. Variables are normalized by $\overline{\rho} u_\tau^{*3}/z_\tau^*$ and plotted in semilocal scale z^*. Here, the ZPG profiles are extracted from Location 1, while all other profiles are from Location 2.

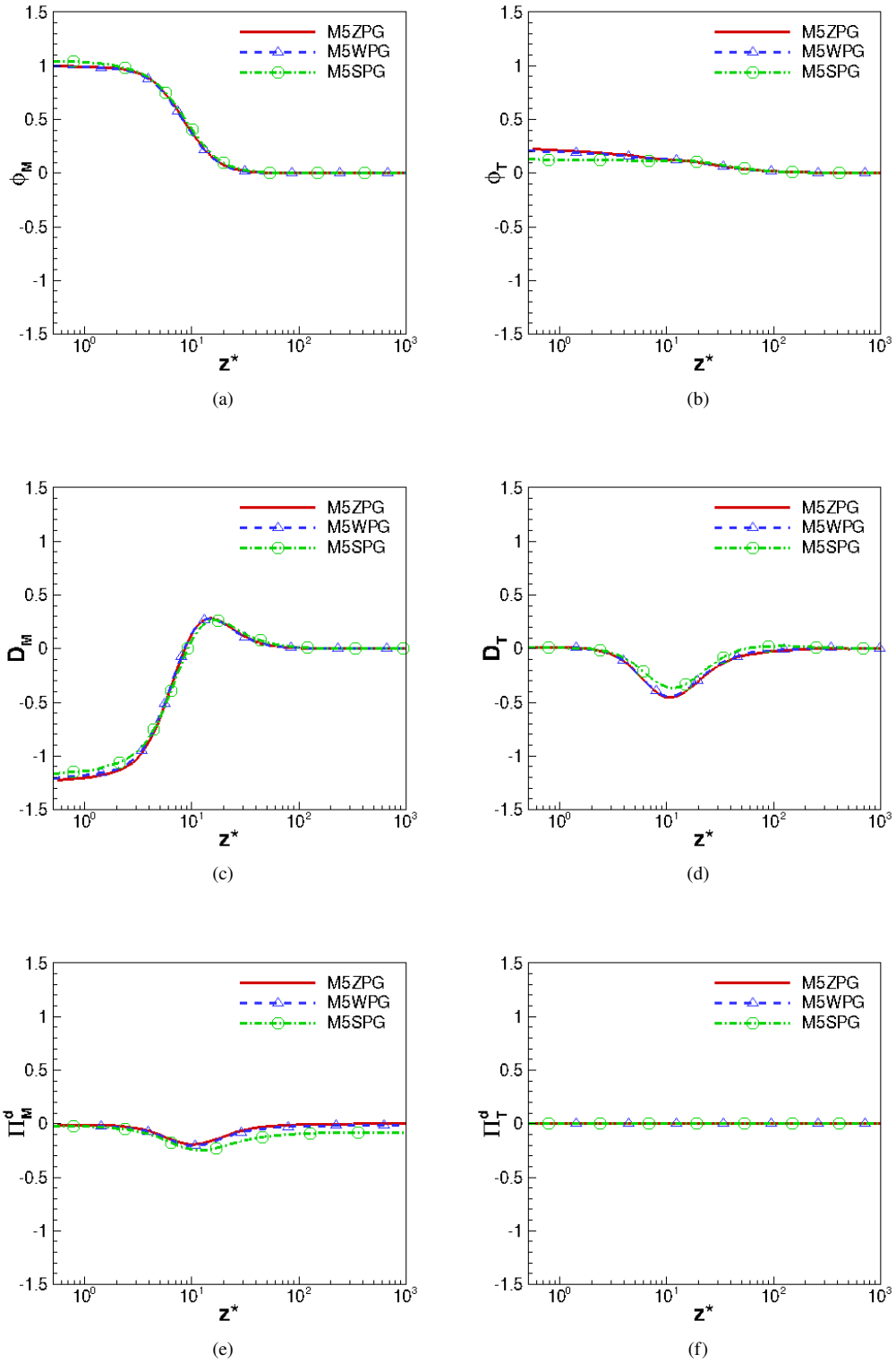

Fig. 8 The internal energy budget $\widetilde{e} = c_v\widetilde{T}$ of DNS cases with varied pressure gradient: (a) mean viscous dissipation ϕ_m, (b) turbulent viscous dissipation ϕ_t, (c) molecular heat flux gradient D_M, (d) turbulent heat flux gradient D_T, (e) mean pressure dilation Π_M^d , (f) turbulent pressure dilation Π_T^d. Variables are normalized by $\overline{\rho}u_\tau^{*3}/z_\tau^*$ and plotted in semilocal scale z^*. Here, the ZPG profiles are extracted from Location 1, while all other profiles are from Location 2.

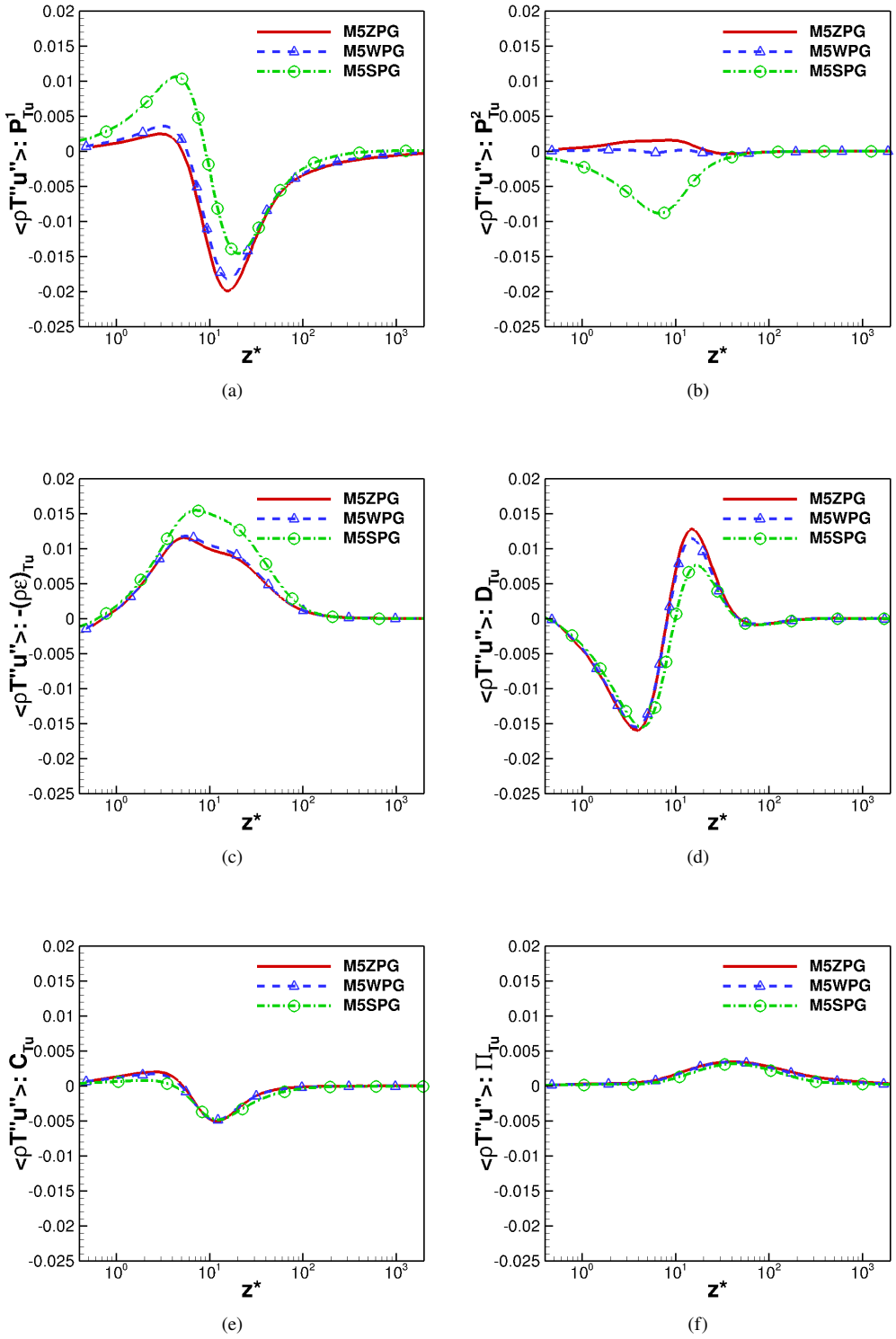

Fig. 9 Comparisons of streamwise heat flux budget terms for DNS cases with varied pressure gradient: (a) the first production term P^1_{Tu}, (b) the second production term P^2_{Tu}, (c) the turbulent viscous-thermal dissipation term $-\overline{\rho}\epsilon_{Tu}$, (d) the turbulent viscous-thermal transport term D_{Tu}, (e) the compressibility terms C_{Tu}, (f) the "pressure-scrambling" term Π_{Tu}. Variables are normalized by $\overline{\rho}u^{*2}_{\tau}\widetilde{T}/z^*_{\tau}$ and plotted in the semilocal scale z^*. The ZPG profiles are extracted from Location 1, while all other profiles are from Location 2.

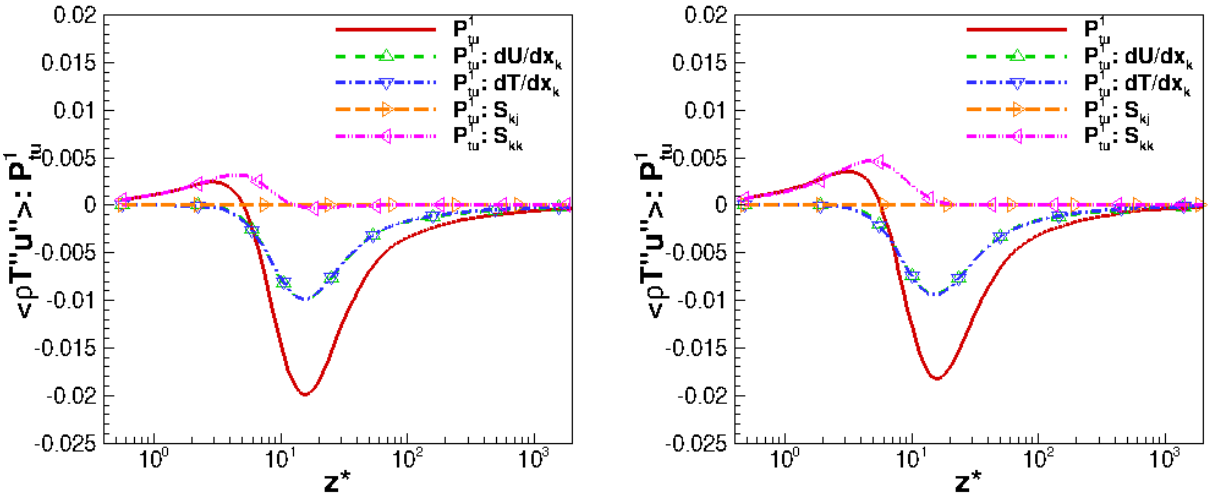

(a) Case M5ZPG

(b) Case M5WPG

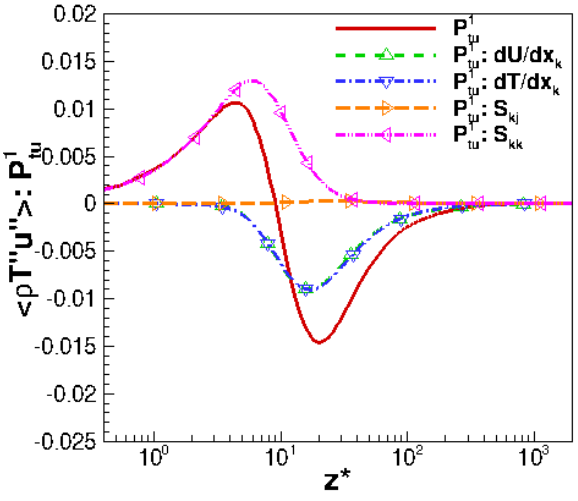

(c) Case M5SPG

Fig. 10 Decomposition of the production term P^1_{Tu} of the streamwise turbulent heat flux budget for (a) Case M5ZPG, (b) Case M5WPG, and (c) Case M5SPG. Variables are normalized by $\overline{\rho} u_\tau^{*2} \widetilde{T}/z_\tau^*$ and plotted in the semilocal scale z^*. Here, the ZPG profiles are extracted from Location 1, while all other profiles are from Location 2.

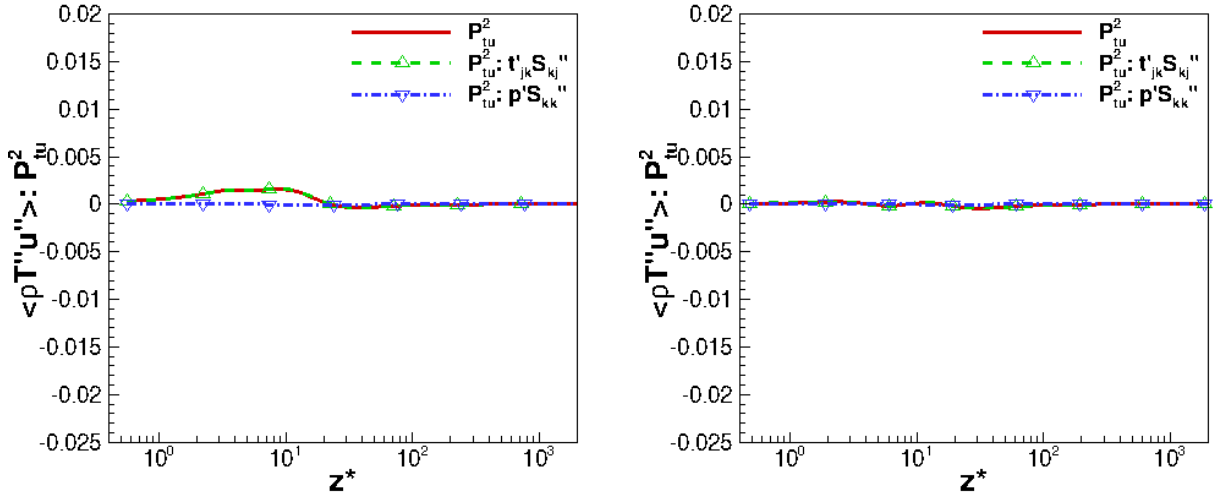

(a) Case M5ZPG

(b) Case M5WPG

(c) Case M5SPG

Fig. 11 Decomposition of the production term P^2_{Tu} of the streamwise turbulent heat flux budget for (a) Case M5ZPG, (b) Case M5WPG, and (c) Case M5SPG. Variables are normalized by $\overline{\rho} u^{*2}_\tau \widetilde{T}/z^*_\tau$ and plotted in the semilocal scale z^*. The ZPG profiles are extracted from Location 1, while all other profiles are from Location 2.

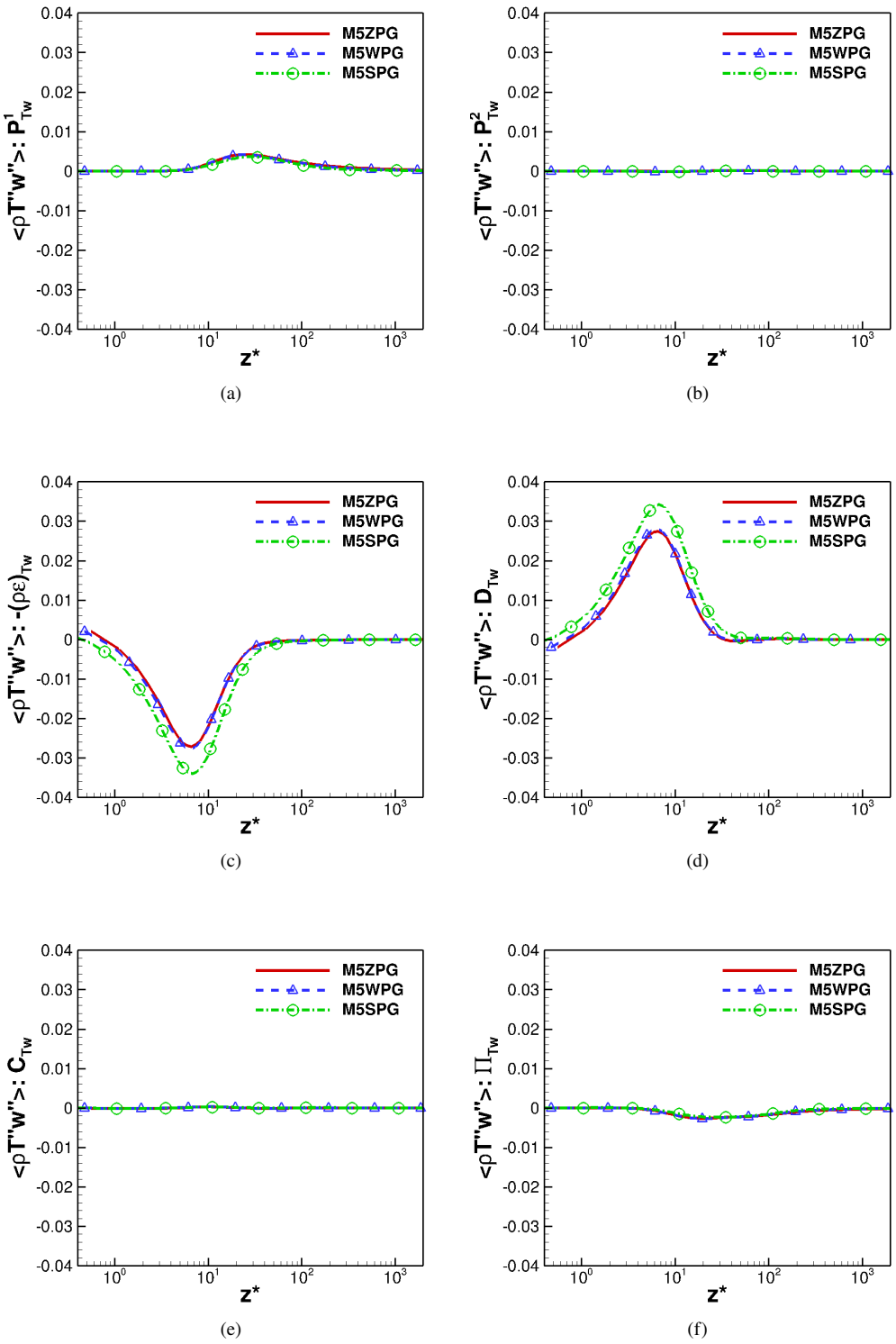

Fig. 12 Comparisons of the wall-normal heat flux budget terms for DNS cases with varied pressure gradient: (a) the first production term P^1_{Tw}, (b) the second production term P^2_{Tw}, (c) the turbulent viscous-thermal dissipation term $-\overline{\rho}\epsilon_{Tw}$, (d) the turbulent viscous-thermal transport term D_{Tw}, (e) the compressibility terms C_{Tw}, (f) the "pressure-scrambling" term Π_{Tw}. Variables are normalized by $\overline{\rho}u^{*2}_{\tau}\widetilde{T}/z^*_{\tau}$ and plotted in the semilocal scale z^*. The ZPG profiles are extracted from Location 1, while all other profiles are from Location 2.

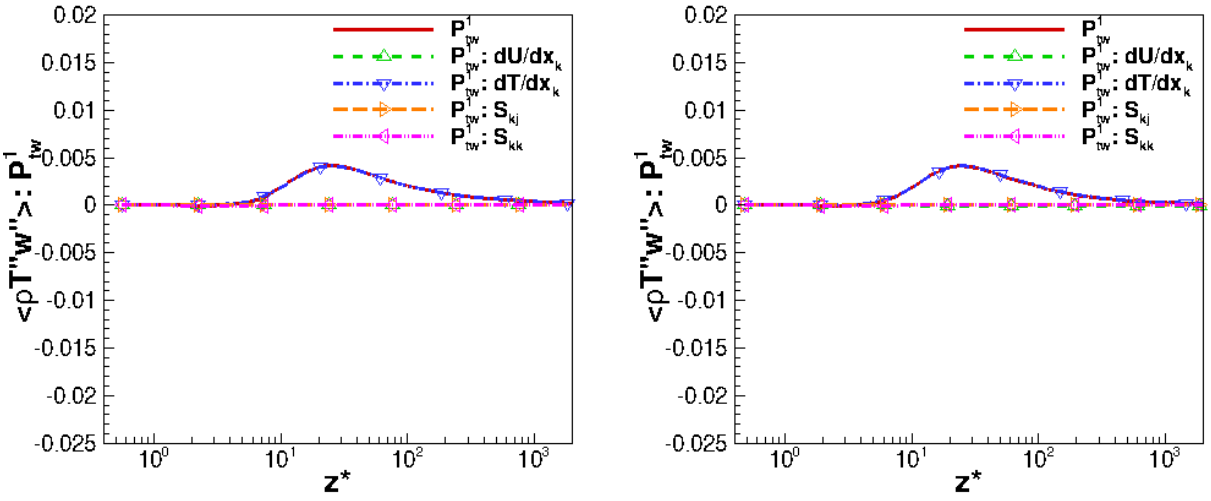

(a) Case M5ZPG

(b) Case M5WPG

(c) Case M5SPG

Fig. 13 Decomposition of the production term P^1_{Tw} of the wall-normal turbulent heat flux budget for (a) Case M5ZPG, (b) Case M5WPG, and (c) Case M5SPG. Variables are normalized by $\overline{\rho}u^{*2}_\tau\widetilde{T}/z^*_\tau$ and plotted in the semilocal scale z^*. Here, the ZPG profiles are extracted from Location 1, while all other profiles are from Location 2.